

## Technical Note

# Differential Subsampling With Cartesian Ordering (DISCO): A High Spatio-temporal Resolution Dixon Imaging Sequence for Multiphasic Contrast Enhanced Abdominal Imaging

Manojkumar Saranathan, PhD,<sup>1\*</sup> Dan W. Rettmann, BS,<sup>2</sup> Brian A. Hargreaves, PhD,<sup>1</sup> Sharon E. Clarke, MD, PhD,<sup>1</sup> and Shreyas S. Vasanawala, MD, PhD<sup>1</sup>

**Purpose:** To develop and evaluate a multiphasic contrast-enhanced MRI method called Differential Sub-sampling with Cartesian Ordering (DISCO) for abdominal imaging.

**Materials and Methods:** A three-dimensional, variable density pseudo-random *k*-space segmentation scheme was developed and combined with a Dixon-based fat-water separation algorithm to generate high temporal resolution images with robust fat suppression and without compromise in spatial resolution or coverage. With institutional review board approval and informed consent, 11 consecutive patients referred for abdominal MRI at 3 Tesla (T) were imaged with both DISCO and a routine clinical three-dimensional SPGR-Dixon (LAVA FLEX) sequence. All images were graded by two radiologists using quality of fat suppression, severity of artifacts, and overall image quality as scoring criteria. For assessment of arterial phase capture efficiency, the number of temporal phases with angiographic phase and hepatic arterial phase was recorded.

**Results:** There were no significant differences in quality of fat suppression, artifact severity or overall image quality between DISCO and LAVA FLEX images ( $P > 0.05$ , Wilcoxon signed rank test). The angiographic and arterial phases were captured in all 11 patients scanned using the DISCO acquisition (mean number of phases were two and three, respectively).

**Conclusion:** DISCO effectively captures the fast dynamics of abdominal pathology such as hyperenhancing hepatic lesions with a high spatio-temporal resolution. Typically,  $1.1 \times 1.5 \times 3$  mm spatial resolution over 60 slices was achieved with a temporal resolution of 4–5 s.

**Key Words:** dynamic contrast enhanced MRI; tumor imaging; time resolved imaging; Dixon fat-water separation

**J. Magn. Reson. Imaging 2012;35:1484–1492.**

© 2012 Wiley Periodicals, Inc.

MULTI-PHASIC CONTRAST enhanced MRI (CEMRI) is commonly used for detection and characterization of primary and metastatic lesions in the abdomen and pelvis. However, compromises are often made between temporal and spatial resolution. A high spatial resolution is required to characterize lesion morphology and relationship to adjacent structures whereas a high temporal resolution is required to accurately characterize and/or quantify contrast uptake as well as to capture the arterial phase of enhancement. In hepatic imaging in particular, the late arterial phase is critical, particularly for tumors such as hepatocellular carcinoma (HCC) and hypervascular metastases. These lesions often exhibit brief arterial phase enhancement and potentially become iso-intense with the liver on subsequent portal venous and equilibrium phase images. For contrast-enhanced abdominal imaging applications in a clinical setting, a T1-weighted three-dimensional (3D) RF spoiled gradient recalled echo (SPGR) sequence with fat suppression is still the most commonly used imaging method, referred to as LAVA/VIBE/THRIVE by three of the major manufacturers (General Electric/Siemens/Philips). The temporal resolution is typically on the order of 15–20 s for adequate spatial resolution and coverage.

Various methods have been proposed to address the spatio-temporal resolution tradeoff in MRI. Some of the earlier keyhole-based methods (1,2) suffered from increased blurring and ghosting artifacts in regions where rapid dynamic changes occur, often the regions of high clinical interest (2). Generalized series modeling methods like RIGR or TRIGR (3,4) can help overcome this problem by using more sophisticated algorithms to extrapolate the missing data but require

<sup>1</sup>Department of Radiology, Stanford University, Stanford, California, USA.

<sup>2</sup>Applied Science Laboratory, GE Healthcare, Rochester, Minnesota, USA.

Contract grant sponsor: NIH; Contract grant numbers: R01-EB009055, P41-RR009784.

\*Address reprint requests to: M.S., Department of Radiology, Lucas Center, MC 5488, Stanford University, Stanford, CA 94305. E-mail: manojksar@stanford.edu

Received October 11, 2011; Accepted January 9, 2012.

DOI 10.1002/jmri.23602

View this article online at [wileyonlinelibrary.com](http://wileyonlinelibrary.com).

solution of large systems of equations, introducing instability and noise amplification. Several  $k$ - $t$  segmentation based time resolved imaging schemes have been proposed and demonstrated but have mostly been confined to high spatio-temporal resolution MR angiography (MRA). Time Resolved Imaging of Contrast KineticS (TRICKS) (5) and Cartesian Acquisition with Projection Reconstruction like sampling (CAPR) (6) segment elliptically ordered 3D  $k$ -space (7) into annular or radial regions and time interleave the acquisition of central and peripheral  $k$ -space regions to achieve temporal acceleration. Highly constrained back projection (HYPR) (8) imaging uses radial undersampling and a composite image to constrain the reconstruction of the subsampled data and eliminate streaking artifacts. Undersampled projection reconstruction imaging with  $k$ -space weighted image combination (KWIC) has been demonstrated in breast imaging by Dougherty et al (9). Parallel imaging techniques (10–12) have also shown considerable potential in improving spatio-temporal resolution, often in conjunction with these other methods.

In addition to high spatio-temporal resolution, uniform fat suppression can be critical for lesion conspicuity as well as for avoiding inadvertent water excitation. This is even more relevant at higher field strengths where fat suppression can be challenging due to more heterogeneous  $B_1$ . Conventional fat suppression techniques apply inversion or saturation pulses centered on the lipid resonance followed by acquisition of multiple lines of  $k$ -space to restrict scan time increase. Recently, variants of the in-phase/out-of-phase method originally proposed by Dixon (13)—the 3-point Dixon based IDEAL (Iterative Decomposition of water and fat with Echo Asymmetry and Least-squares estimation) (14) and the 2-point based MEDAL (Multi-Echo with 2-Point Dixon Reconstruction for Decomposition of Aqua/Lipid) (15)—have been shown to be robust for fat-water separation, in the presence of  $B_0$  inhomogeneity. The elimination of magnetization preparation pulses provides these Dixon-based methods complete flexibility in the order of  $k$ -space acquisition, and in particular enables combination with elliptical centric or other novel nonsequential  $k$ -space ordering approaches. However, the temporal resolution of these sequences for abdominal imaging is on the order of 15–20 s (16,17), making them suboptimal for visualization of fast enhancing lesions.

Recently, TRICKS (5) was applied to liver DCEMRI in conjunction with a 2-point Dixon based fat suppression method (18). In this acquisition approach called META,  $k$ -space was divided into elliptical regions and the central  $k$ -space regions were acquired more frequently than the peripheral regions. At each reconstructed time frame, missing  $k$ -space data were estimated using linear interpolation from previous and succeeding time frames. One drawback of this method was the interpolation across successive breathholds, which could lead to ghosting artifacts due to inconsistent breathholding. This could partly be addressed using higher channel-count receive array coils, which would enable higher parallel imaging acceleration and better view sharing schemes.

In this study, we develop and demonstrate clinical feasibility of a new high spatio-temporal resolution DCEMRI technique, referred to as DISCO (Differential Sub-sampling with Cartesian Ordering), that combines a dual-echo SPGR sequence with pseudo-random variable density  $k$ -space segmentation and a view sharing reconstruction. DISCO samples an elliptically ordered central  $k$ -space region every time, and sub-samples the outer regions with pseudo-random segmentation such that the aliasing artifacts from subsampling are rendered somewhat incoherent. Robust fat suppression is achieved using a 2-point Dixon fat-water reconstruction algorithm, which is completely compatible with the irregular  $k$ -space ordering scheme as described above.

## MATERIALS AND METHODS

### Pulse Sequence and Reconstruction:

A variable density  $k$ -space undersampling strategy was developed to generate a pseudo-random distribution of  $k$ -space points. All points in  $k_y$ - $k_z$  space are first sorted in the order of increasing  $k_r = \sqrt{(k_y^2 + k_z^2)}$ . This elliptically ordered  $k_y$ - $k_z$  space is segmented into  $N$  annular regions and each region  $i$  is subsampled by a factor of  $S_i$  (typically  $S_i \geq i$ ) with the central region being fully sampled and the outer regions being progressively subsampled by retaining every  $S_i^{\text{th}}$  sample (again in order of increasing  $k_r$  within the region). For each region,  $S_i$  different sampling patterns can be generated by staggering the starting sample from 1 through  $S_i$ . Note that all  $k$ -space points are still confined to a Cartesian grid to retain the advantages of Cartesian image reconstruction. We call this method Differential Sub-sampling with Cartesian Ordering or DISCO.

The temporal footprint (i.e., total time extent of samples used to reconstruct a temporal phase) was minimized by nearest-neighbor view sharing of the undersampled views. View sharing was restricted to nearest neighbors *and* to  $k$ -space segments acquired within the same breathhold, minimizing temporal blurring and motion mis-registration. For  $N = 2$  and  $S_i = i$ , the region schedule is  $AB_1AB_2AB_3AB_1\dots$  where  $X_i$  refers to the under-sampled subset of the fully sampled region  $X$  (Fig. 1b). Because each sub-region is elliptically ordered in increasing  $k_r$ , points are traversed smoothly and eddy current artifacts that can accrue due to true stochastic sampling are mitigated while still imparting a degree of “randomness”, when viewed in  $k_y$ - $k_z$  space.

The DISCO  $k$ -space segmentation scheme was incorporated into a dual-echo bipolar-readout 3D SPGR sequence depicted in Figure 1c. A 2-point Dixon reconstruction with a region-growing based fat-water separation method proposed in Ma (15) was used for fat-water separation. The use of high receiver bandwidths ( $\pm 167$  kHz) enabled the acquisition of opposed-phase and in-phase echoes at approximately 1.2 ms and 2.4 ms (optimal for 3T) in a single TR, greatly reducing scan times and enabling reliable fat-water separation. Self-calibrated hybrid space parallel

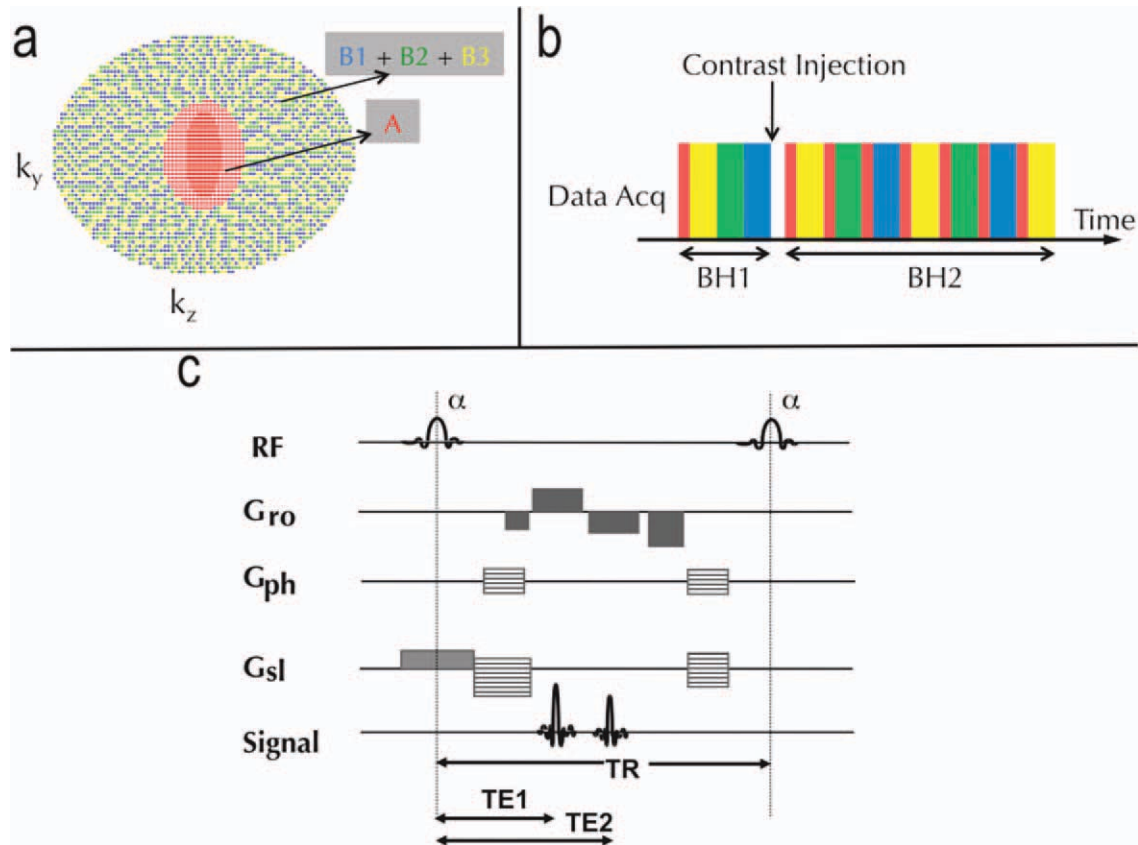


**Figure 1.** The DISCO *k*-space segmentation scheme (a), acquisition schedule (b) and the pulse sequence diagram of the proposed DISCO scheme (c). The central red region is acquired every time and the outer pseudorandom subsampled regions (blue, green, yellow) are interleaved. The in-phase and the opposed-phase echoes are both acquired in a single TR of a fast spoiled gradient recalled echo sequence and the pulse parameters adjusted such that TE1 and TE2 are approximately 1.1 ms and 2.2 ms at 3T field strength.

imaging (ARC) enabled the use of two dimensional acceleration (along  $k_y$  and  $k_z$ ) (19). Following nearest neighbor view-sharing and ARC parallel imaging reconstruction, full *k*-space in-phase and opposed-phase complex images were available at each reconstructed time point. These were then passed through the Dixon reconstruction algorithm with a phase correction as described in Ma (15) to yield fat-only and water-only image volumes at each reconstructed phase. All reconstruction algorithms were implemented on-line on the vendor-supplied (GE Healthcare) eight-processor (2.4 GHz) cluster to minimize image reconstruction latency. Each temporal phase took approximately 60 s to reconstruct after the acquisition of the requisite *k*-space data.

## EXPERIMENTS

### Simulations and Phantom Experiments

MATLAB (MathWorks, Natick, MA) simulations were used to compute the Point Spread Function (PSF) of sub-sampled TRICKS, CAPR, and DISCO trajectories. For each trajectory, a central *k*-space region (A) and one peripheral region—a ring in the case of TRICKS, a set of spokes in the case of CAPR, a set of pseudo-randomly distributed points confined to an annulus

in the case of DISCO—was used to generate the PSF. The size of the central *k*-space region and the total number of points was kept constant for all three trajectories. Using a  $120 \times 120$  matrix, the size of the central A region was 1600 and the peripheral B region 2800 for all three cases.

To evaluate the impact of PSF on image quality, a doped resolution phantom was used to compare the effect of motion on the three trajectories. Halfway through a 25-s scan, the phantom was moved by 5 mm to simulate motion that could, for example, arise from loss of breathholding. The scan parameters used were identical to the human subject scans detailed below with the exception that parallel imaging was not used. For both the phantom experiments and PSF simulations above, a single A region (fraction 0.16) and three B regions with equal number of *k*-space points (fraction 0.28) were used to span full *k*-space, with the B regions being elliptical annuli for TRICKS, radial sectors for CAPR and pseudorandom regions for DISCO.

### Human Subjects

Human experiments were conducted following institutional review board approval and informed consent. To evaluate DISCO's motion robustness and reduced temporal footprint, healthy volunteers were asked to

Table 1  
Scoring Criteria for Image Comparisons Between DISCO and LAVA FLEX

Score	Overall image quality	Artifact severity	Quality of fat suppression
0	Non-diagnostic	Uninterpretable images	Complete failure of fat suppression
1	Only large <i>and</i> intensely enhancing lesions would be detectable	Large lesions are still detectable	Large regional fat-water swaps due to failure of the Dixon algorithm
2	Only large or intensely enhancing lesions would be detectable	Artifacts limiting detection of small lesions	Regional fat-water failures but still interpretable
3	Image quality for detection of small subtly enhancing lesions	Subtle artifacts but diagnostic	Minimal failures in image periphery
4	No artifacts and minimal image noise	No noticeable artifacts	Perfect fat-water separation

hold their breath at slightly different positions in the first and second end-inspiration breathholds and two sets of images reconstructed: (i) view sharing *within* a breathhold and (ii) *across* breathholds. Imaging was performed on a GE 3T MR750 system (GE Healthcare, Waukesha, WI) with the following parameters: 12° flip,  $\pm 167$  kHz bandwidth, TR/TE<sub>1</sub>/TE<sub>2</sub> 4.1/1.2/2.4 ms, 320 × 224 matrix, 30–35 cm FOV, 3 mm slice thickness, 60 slices, ARC 2 × 2 outer acceleration. Using a net acceleration factor of 3.4 (to account for ARC calibration), the total k<sub>y</sub>-k<sub>z</sub> points is  $\sim 3000$ , assuming an elliptical *k*-space region. This yields an A region size of 0.16\*3000 = 480 and three B regions of size of 0.28\*3000 = 840. The total number of points for each phase is hence 1320 yielding  $\sim 5.2$  s temporal resolution.

After validation experiments in volunteers, eleven consecutive patients referred for abdominal MRI were recruited into the study. A 32-channel torso array coil optimized for high acceleration factors was used with the upper 19 elements enabled for the data acquisition and reconstruction of the abdominal scans. Following localizer scans and axial fat-suppressed fast spin echo T<sub>2</sub> weighted imaging, DISCO was run to acquire a full *k*-space breathheld data set, which also served as a pre-contrast reference phase. For contrast enhanced imaging, gadoxetate was used in three patients and gadobenate in eight patients. After injection of a single dose of gadolinium contrast (0.2 mL/kg for gadobenate, 0.1 mL/kg for gadoxetate) at 2 cc/s followed by 20-mL saline chaser at the same rate, the remaining *k*-space data were acquired as shown in Figure 1a. This second 24–28 s breathhold typically yielded 6–7 temporal phases with a temporal resolution of 4–5 s. The timing for this dynamic breathhold was fixed at 15 s following contrast injection to minimize any possibility of early arrival of contrast. For image quality comparisons, a 3D SPGR with 2-point Dixon reconstruction (3D LAVA FLEX) scan was acquired in an immediately subsequent breathhold with the same sequence parameters including parallel imaging acceleration factors. The temporal resolution of this sequence was  $\sim 14$  s. All breathhold image acquisitions including the scout scans were performed during end-inspiration to maximize patient comfort.

### Data Analysis

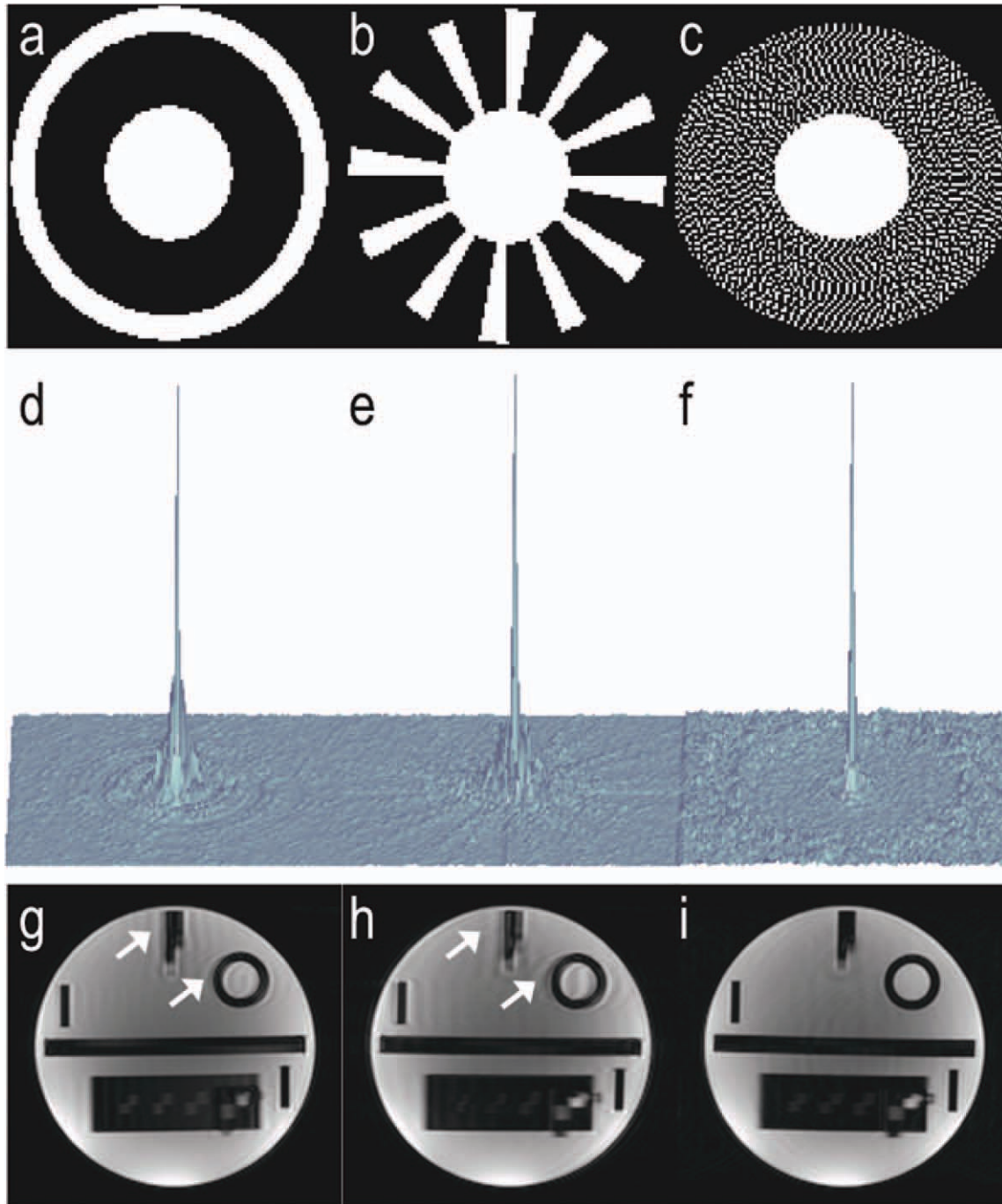
In all patients, the 3D LAVA FLEX scan acquired immediately after DISCO was used for comparing overall

image quality, severity of artifacts, and quality of fat suppression. The last DISCO phase was used for the comparisons to use a temporal phase closest to that of the LAVA FLEX scan. The number of angiographic and arterial temporal phases that were captured by the DISCO acquisition were also recorded. The criteria for designating a temporal phase as an angiographic phase were both a bright hepatic artery and no portal vein enhancement. The criteria for a hepatic arterial phase were some portal venous enhancement that was less intense than that of the hepatic artery, as well as no enhancement of hepatic veins. The images were randomized and graded for quality of liver delineation on a scale of 0–4 by consensus review of two experienced board-certified radiologists. The categories for image scoring were overall image quality, artifact severity and quality of fat suppression. Table 1 summarizes the criteria and the scoring scale. A non-parametric Wilcoxon signed rank test was used to compare qualitative ordinal image scores.

### RESULTS

Figure 2 compares subsampling point spread functions obtained from simulations of TRICKS, CAPR, and DISCO *k*-space segmentation schemes (a–c) for the same total number of sampled points. Note the significant dispersal of ghosting energy in DISCO (f) compared with that of TRICKS (d) and CAPR (e) due to the pseudo-random nature of sampling in DISCO suggesting that artifacts arising due to view sharing and potential signal discontinuities between regions being shared may be much more dispersed in DISCO compared with TRICKS or CAPR. Comparable sections from a 3D acquisition on a resolution phantom, where the phantom was displaced by 5 mm midway through the scan are shown in (g–i) for the three different *k*-space segmentation schemes. Note that the artifacts (arrows) are stronger and more coherent in TRICKS and CAPR (g,h) compared with DISCO (i), agreeing with the point spread function simulations.

Comparable slices from the first temporal phase of the second breathhold of a DISCO scan on a healthy human subject with view sharing spanning across two end inspiration breathholds (a) and view sharing restricted to within the second end inspiration breathhold (b) are shown in Figure 3. Note that the ghosting artifacts in (a) (white arrow) due to mis-registration of the first and second breathholds, are completely



**Figure 2.** The  $k_y$ - $k_z$  segmentation scheme for TRICKS (a), CAPR (b), and DISCO (c) and the corresponding subsampled point spread functions (d-f). Note that the point spread function for DISCO (f) shows significantly reduced coherent artifacts around the main lobe and in the periphery compared with that of TRICKS (d) and CAPR (e). Comparable sections from a 3D acquisition on a resolution phantom, where the phantom was displaced by 5 mm midway through the scan are shown in (g-i). Note that the artifacts (arrows) are stronger and more coherent in TRICKS and CAPR (g,h) compared with DISCO (i), agreeing with the point spread function simulations. [Color figure can be viewed in the online issue, which is available at [wileyonlinelibrary.com](http://wileyonlinelibrary.com).]

eliminated in (b), allowing the use of end-inspiration breathholding in DISCO.

Figure 4 shows box-whisker plots of radiologist image score distribution using overall image quality, artifact severity and degree of fat suppression as scoring criteria of the proposed DISCO method and conventional 3D LAVA FLEX sequence. There were no significant differences between the two techniques ( $P >$

0.05) for any of the scoring criteria. At least one angiographic phase and one arterial phase were captured in each of the 11 cases (mean number of angiographic and arterial phases identified— $1.91 \pm 0.8$  and  $3.27 \pm 1.5$ , respectively) attesting to the high temporal resolution of the proposed DISCO technique.

Representative results with eight temporal phases ( $\sim 4$  s temporal resolution) obtained on a 67-year-old

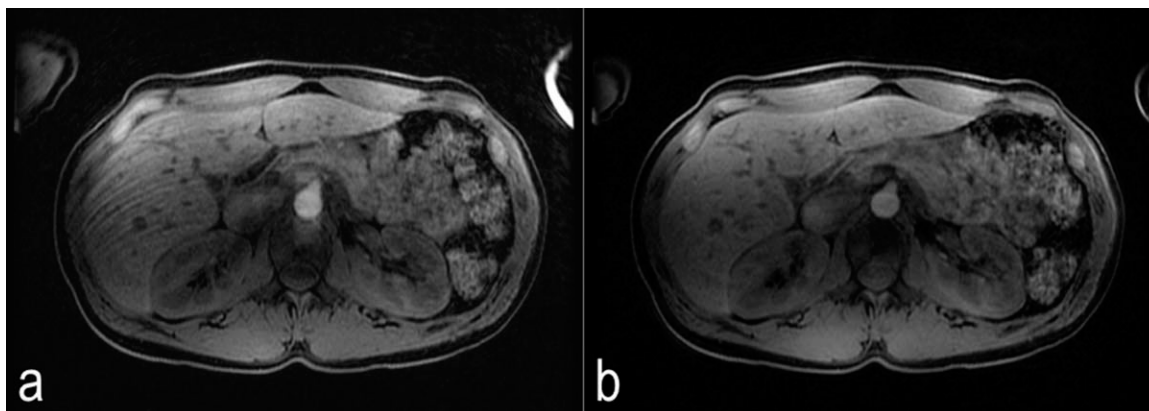


**Figure 3.** Comparable slices from the first temporal phase of the second breathhold of a DISCO scan on a healthy human subject with view sharing spanning across two end inspiration breathholds (a) and view sharing restricted to within each breathhold (b). Note that the motion artifacts in (a) (liver) are eliminated in (b).

male with two foci of likely hepatocellular carcinoma are shown in Figure 5. Non-contrast-enhanced fully sampled data was obtained in one breathhold (a), followed by a second breathhold of seven DISCO dynamic contrast enhancement phases (b–h) showing first arteries (black arrow), tumors (nondashed and dashed white arrow), portal veins (solid grey arrow), and hepatic veins (thin long black arrow) enhancing with a single-dose gadoxetate injection. Note that the tumors show hyper-enhancement on only two temporal phases, mostly at the time the portal vein has its first blush of contrast (thin dashed black arrow in e). Also note that by this time, contrast has already washed out from the hepatic arteries.

Another multiphasic DISCO acquisition from a 53-year-old female with a likely hepatocellular carcinoma is shown in Figure 6. Non-contrast-enhanced fully sampled data was acquired in one breathhold (a) followed by a second breathhold of six DISCO dynamic contrast enhancement phases with  $\sim 4$  s temporal resolution (b–g) showing an enhancing tumor (white arrow) and an adjacent transient hepatic intensity difference (dashed white arrow) with a single-dose gadobenate injection. Note regions of hyper-enhancement of the tumor are rapidly reaching same signal intensity as background liver (black arrows in g). The fully sampled LAVA FLEX data obtained in a third breathhold a few seconds later (h) shows comparable image quality.

## DISCUSSION

Contrast enhanced body MRI applications, especially hepatic and renal imaging, require high spatio-temporal resolution to reliably capture the angiographic and arterial phases with robust fat suppression and minimal motion blurring/artifacts. The proposed DISCO pulse sequence combining a variable density pseudo-random  $k$ -space segmentation scheme, view sharing, a 2-point Dixon-based fat-water separation, and 2D parallel imaging using ARC provided excellent fat suppression at 3T where conventional fat saturation techniques are often suboptimal. It also provided a high spatio-temporal resolution for excellent visualization

of structures with rapid contrast enhancement and washout and visualization of the angiographic and arterial phases in all 11 patient cases scanned. Approximately 6–7 phases were reconstructed from data acquired in a 28–30 s end-inspiration breathhold, resulting in a temporal resolution of  $\sim 4$  s with  $\sim 1 \times 1.5 \times 3$  mm spatial resolution. The use of a Dixon-based fat-water separation scheme was critical to enable the use of a pseudo random  $k$ -space segmentation scheme because conventional fat suppression schemes require sequential or linearly segmented  $k$ -space for optimal performance. The image quality of the DISCO images were comparable to and statistically no worse than the 3D LAVA FLEX despite higher frame rates that captured arterial and angiographic phases in all 11 cases and enabled clear visualization of hypervascular tumors.

One advantage of our  $k$ -space segmentation and view sharing scheme over the previously proposed META technique (18) is its immunity to breathhold mismatching. In Saranathan et al (18),  $k$ -space data was linearly interpolated across multiple breathholds necessitating the use of end-expiratory breathholding,

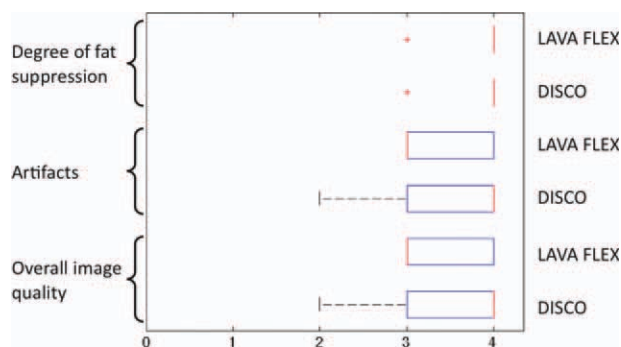


**Figure 4.** Distribution of scores from radiologist rankings in overall image quality, artifact severity and quality of fat suppression between DISCO and conventional LAVA FLEX acquisitions. There were no significant differences found amongst the two methods for all three criteria ( $P > 0.05$ ). [Color figure can be viewed in the online issue, which is available at [wileyonlinelibrary.com](http://wileyonlinelibrary.com).]

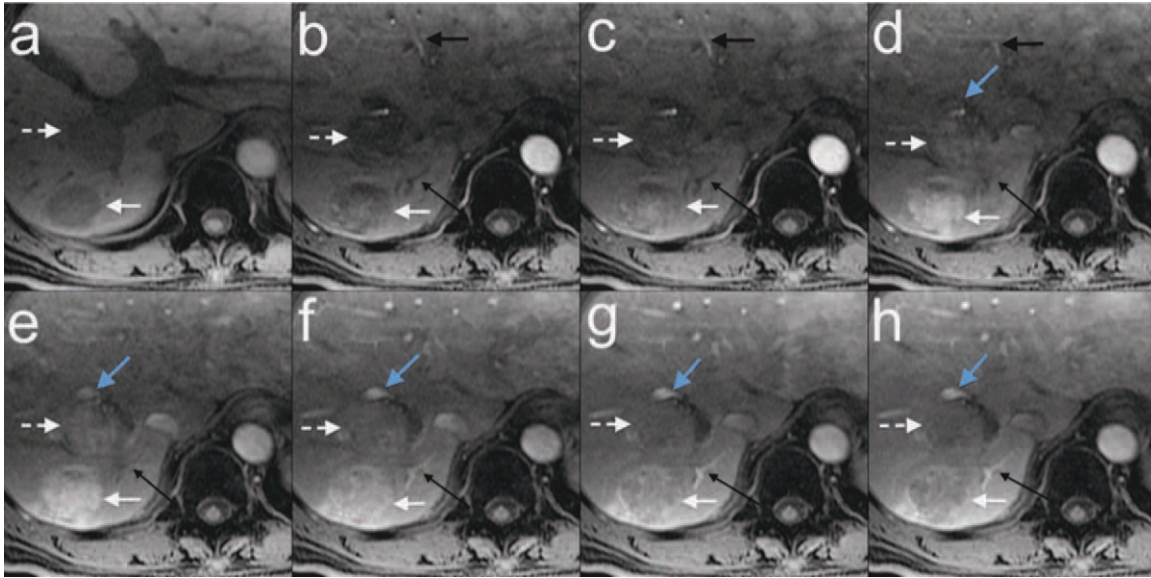


**Figure 5.** 67 year old male with two foci of likely hepatocellular carcinoma. Non-contrast-enhanced fully sampled data obtained in one breathhold (**a**), followed by a second breathhold of seven DISCO contrast enhancement phases (**b-h**) with  $\sim 4$  s temporal resolution showing first arteries (black arrow), tumors (nondashed and dashed white arrow), portal veins (solid grey arrow), and hepatic veins (thin long black arrow) enhancing with a single- dose gadoxetate injection. Note that the tumors show hyper-enhancement on only two phases, mostly at the time the portal vein has its first blush of contrast (thin dashed black arrow in e). Also note that by this time, contrast has already washed out from the hepatic arteries. [Color figure can be viewed in the online issue, which is available at [wileyonlinelibrary.com](http://wileyonlinelibrary.com).]

which is challenging for many patients. While end-expiratory breathholding is more consistent, it is still possible to have mismatches between successive breathholds, resulting in motion artifacts. DISCO eliminates this by restricting the view sharing to

within a breathhold and thereby reducing its temporal footprint compared with META. This can be seen in Figure 3 where the *across* breathhold reconstruction resulted in artifacts compared with the *within* breathhold reconstruction. Furthermore, the pseudo-

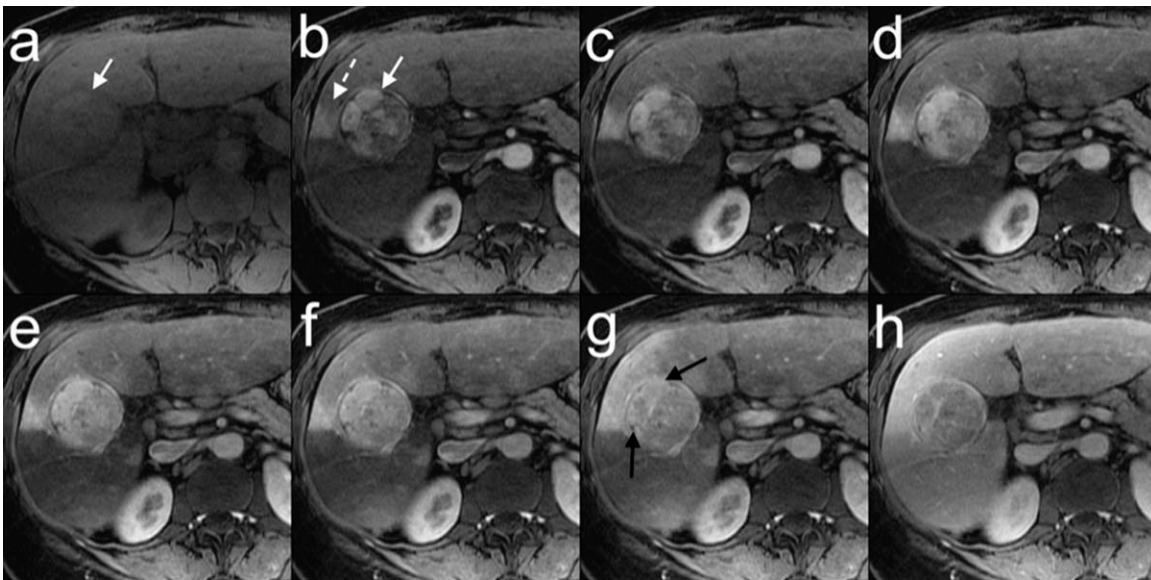


**Figure 6.** A 53-year-old female with a likely hepatocellular carcinoma. Non-contrast-enhanced data acquired in one breathhold (**a**) followed by a second breathhold of six DISCO contrast enhancement phases (**b-g**) with  $\sim 4$  s temporal resolution showing enhancing tumor (white arrow) and a transient hepatic intensity difference (dashed white arrow) with a single-dose gadobentate injection. Note regions of hyper-enhancement of the tumor are rapidly reaching same signal intensity as background liver (black arrows in g). Fully sampled LAVA FLEX data obtained in a third breathhold a few seconds later (**h**) shows comparable image quality.

random nature of outer  $k$ -space in the DISCO  $k$ -space segmentation scheme disperses motion artifacts in much the same way as undersampling artifacts are dispersed in radial imaging as illustrated in the PSF simulations of Figure 2. The use of higher channel count surface coils could enable META acquisition with higher acceleration than was reported in Sarathan et al (18) but the limitations of a linear interpolation based reconstruction method would still require that some of the  $k$ -space data be shared between breath holds or reduce the total number of dynamic phases acquired compared with nearest-neighbor viewsharing.

The DISCO  $k$ -space segmentation bears similarity to the recently proposed TWIST scheme (20), which has been applied to peripheral MRA (21), renal imaging (22) and more recently to breast DCEMRI (23). DISCO uses a variable density undersampling scheme, i.e.,  $k$ -space is progressively undersampled away from the center and is capable of achieving higher subsampling rates than the spiral in-spiral out scheme of TWIST. Unlike TWIST, where the  $k$ -space radius  $k_r$  of the acquired  $k$ -space points oscillates as a function of time within each temporal phase, it monotonically increases from the center outward in DISCO, perhaps making it better suited for capture of contrast kinetics, akin to true elliptical centric  $k$ -space ordering. Furthermore, the work of Herrmann et al (23) used a mask subtraction scheme in the breast to eliminate fat, which is suboptimal for breathholding applications. Even in breast imaging with relatively minimal motion, the authors had to resort to a retrospective image registration scheme. The use of Dixon fat-water separation in conjunction with DISCO makes it ideal for applications like breast and liver imaging, where fat suppression is especially challenging due to  $B_0/B_1$  heterogeneity. Recently, Dixon fat-water separation has been shown to be superior to conventional fat suppression in reducing motion artifacts in breast imaging (24).

This preliminary study had some limitations. We studied a small number of patients ( $n = 11$ ) to assess the feasibility and image quality of the DISCO technique. While the last DISCO phase which was temporally close to the LAVA FLEX scan was used for image comparisons, in some cases, they were in different stages of enhancement (late arterial vs. portal venous for example). However, the comparisons were more to evaluate potential artifacts that could be introduced by the DISCO viewsharing scheme rather than features specific to stage of enhancement. A comparison of the arterial phase capture efficiency of the conventional method (3D LAVA FLEX for example) using, say, a cohort of  $n$  successive patients imaged was not possible due to large variations in the protocol parameters of the conventional sequence stemming from the tailoring of imaging parameters by the technologist to individual patient size and predicted breathholding capacity. Using DISCO, the angiographic and arterial phases were captured on each of the 11 cases, spanning an average of two and three temporal phases, respectively. While there were no artifacts introduced due to view sharing compared with the conventional

3D LAVA FLEX scans, some degree of temporal blurring could be expected with view sharing especially in fast enhancing lesions. The inherent pseudo-random sampling of the DISCO trajectory (which results in a relatively incoherent PSF) is compatible with a compressed sensing reconstruction. Future developments would investigate the use of compressed sensing reconstruction techniques to reconstruct a single phase without view sharing. A larger clinical study comparing the DISCO technique to conventional LAVA FLEX as well with alternative reconstruction strategies is currently underway.

Optimizing arterial phase timing for contrast-enhanced MRI can be challenging in hepatic MRI, particularly for lesions such as hepatocellular carcinoma and neuroendocrine metastases which are sometimes visualized briefly during the arterial phase (25). This is particularly relevant when using a contrast agent with a fast vascular clearance such as gadoxetate as illustrated in Figure 5, where the rapid contrast wash-in and wash-out has been effectively captured by the DISCO technique. In addition, the angiographic phase can be of considerable value in planning chemo-embolization procedures for treatment planning to visualize collateral arteries to lesions. Our feasibility study demonstrates some of the advantages of the DISCO technique compared with conventional 3D LAVA FLEX or SPGR imaging including significantly improved efficiency of arterial phase capture, and comparable overall image quality and artifacts. Beyond hepatic imaging, other potential applications of this technique include MR urography, and dynamic contrast enhanced imaging of the breast and prostate.

In conclusion, the DISCO technique allows acquisition of 3D volumes with an effective temporal resolution of 4–5 s while preserving spatial resolution, fat suppression and image quality and its feasibility has been demonstrated in a clinical setting. This technique may help to alleviate some of the variability in the appearance of arterial phase images from examination to examination and thereby allow more confident assessment of interval growth or stability of small enhancing lesions.

## ACKNOWLEDGMENT

The authors thank Dr. Pauline W. Worters for helpful discussions and assistance with the figures.

## REFERENCES

1. van Vaals JJ, Brummer ME, Dixon WT, et al. "Keyhole" method for accelerating imaging of contrast agent uptake. *J Magn Reson Imaging* 1993;3:671–675.
2. Plewes DB, Bishop J, Soutar I, Cohen E. Errors in quantitative dynamic three-dimensional keyhole MR imaging of the breast. *J Magn Reson Imaging* 1995;5:361–364.
3. Liang ZP, Lauterbur PC. An efficient method for dynamic magnetic resonance imaging. *IEEE Trans Med Imaging* 1994;13:677–686.
4. Hanson JM, Liang ZP, Wiener EC, Lauterbur PC. Fast dynamic imaging using two reference images. *Magn Reson Med* 1996;36:172–175.

5. Korosec FR, Frayne R, Grist TM, Mistretta CA. Time-resolved contrast-enhanced 3D MR angiography. *Magn Reson Med* 1996;36:345–351.
6. Madhuranthakam AJ, Hu HH, Barger AV, et al. Undersampled elliptical centric view-order for improved spatial resolution in contrast-enhanced MR angiography. *Magn Reson Med* 2006;55:50–58.
7. Wilman AH, Riederer SJ. Performance of an elliptical centric view order for signal enhancement and motion artifact suppression in breath-hold three-dimensional gradient echo imaging. *Magn Reson Med* 1997;38:793–802.
8. Mistretta CA, Wieben O, Velikina J, et al. Highly constrained backprojection for time-resolved MRI. *Magn Reson Med*. 2006;55:30–40.
9. Dougherty L, Isaac G, Rosen MA, et al. High frame-rate simultaneous bilateral breast DCE-MRI. *Magn Reson Med* 2007;57:220–225.
10. Pruessmann KP, Weiger M, Scheidegger MB, Boesiger P. SENSE: sensitivity encoding for fast MRI. *Magn Reson Med* 1999;42:952–962.
11. Sodickson DK, Manning WJ. Simultaneous acquisition of spatial harmonics (SMASH): fast imaging with radiofrequency coil arrays. *Magn Reson Med* 1997;38:591–603.
12. Vogt FM, Antoch G, Hunold P, et al. Parallel acquisition techniques for accelerated volumetric interpolated breath-hold examination magnetic resonance imaging of the upper abdomen: assessment of image quality and lesion conspicuity. *J Magn Reson Imaging* 2005;21:376–382.
13. Dixon WT. Simple proton spectroscopic imaging. *Radiology* 1984;153:189–194.
14. Reeder SB, Markl M, Yu H, Hellinger JC, Herfkens RJ, Pelc NJ. Cardiac CINE imaging with IDEAL water-fat separation and steady-state free precession. *J Magn Reson Imaging* 2005;22:44–52.
15. Ma J. Breath-hold water and fat imaging using a dual-echo two-point Dixon technique with an efficient and robust phase-correction algorithm. *Magn Reson Med* 2004;52:415–419.
16. Rosenkrantz AB, Mannelli L, Kim S, Babb JS. Gadolinium-enhanced liver magnetic resonance imaging using a 2-point Dixon fat-water separation technique: impact upon image quality and lesion detection. *J Comput Assist Tomogr* 2011;35:96–101.
17. Low RN, Bayram E, Panchal NJ, Estkowski L. High-resolution double arterial phase hepatic MRI using adaptive 2D centric view ordering: initial clinical experience. *AJR Am J Roentgenol* 2010;194:947–956.
18. Saranathan M, Rettmann D, Bayram E, Lee C, Glockner J. Multi-echo time-resolved acquisition (META): a high spatiotemporal resolution Dixon imaging sequence for dynamic contrast-enhanced MRI. *J Magn Reson Imaging* 2009;29:1406–1413.
19. Beatty PJ, Brau AC, Chang S, et al. A method for autocalibrating 2-D accelerated volumetric parallel imaging with clinically practical reconstruction times. In: Proceedings of the 15th Annual Meeting of ISMRM, Berlin, Germany, 2007. (abstract 1749).
20. Vogt FM, Eggebrecht H, Laub G, et al. High spatial and temporal resolution MRA (TWIST) in acute aortic dissection. In: Proceedings of the 15th Annual Meeting of ISMRM, Berlin, Germany, 2007. (abstract 92).
21. Lim RP, Shapiro M, Wang EY, et al. 3D time-resolved MR angiography (MRA) of the carotid arteries with time-resolved imaging with stochastic trajectories: comparison with 3D contrast-enhanced Bolus-Chase MRA and 3D time-of-flight MRA. *AJNR Am J Neuroradiol* 2008;29:1847–1854.
22. Song T, Laine AF, Chen Q, et al. Optimal k-space sampling for dynamic contrast-enhanced MRI with an application to MR renography. *Magn Reson Med* 2009;61:1242–1248.
23. Herrmann KH, Baltzer PA, Dietzel M, et al. Resolving arterial phase and temporal enhancement characteristics in DCE MRM at high spatial resolution with TWIST acquisition. *J Magn Reson Imaging* 2011;34:973–982.
24. Shi K, Zhou K, Niu X, et al. Investigation of motion artifacts associated with fat saturation technique in 3D flash imaging. *Med Phys* 2011;38:4556–4562.
25. Ito K, Fujita T, Shimizu A, et al. Multiarterial phase dynamic MRI of small early enhancing hepatic lesions in cirrhosis or chronic hepatitis: differentiating between hypervascular hepatocellular carcinomas and pseudolesions. *AJR Am J Roentgenol* 2004;183:699–705.